Nuclear Resonance Beamline at ESRF

Rudolf Rüffer and Aleksandr I. Chumakov

European Synchrotron Radiation Facility, BP 220, F-38043 Grenoble Cedex, France

The Nuclear Resonance Beamline at ESRF is dedicated to the excitation of nuclear levels by synchrotron radiation. The sources of radiation and optical elements are optimized to provide an intense, highly monochromatic, collimated and stable X-ray beam of small cross-section at the Mössbauer transition energies between 6 and 30 keV. The set-up of the beamline allows to perform studies in diffraction, small angle scattering, forward scattering and incoherent scattering. Equipment is available to maintain the sample at variable temperature and magnetic field. Fast detectors and timing electronics serve to separate the delayed nuclear scattering from the "prompt" electronic scattering and to measure the time spectra of nuclear radiation with sub-nanosecond resolution. The general lay-out and the parameters of the beamline are reported. Typical domains of applications are discussed and illustrated by first experimental results.

1. Introduction

In the last ten years experiments on the excitation of nuclear levels by synchrotron radiation passed the way from pioneering observations [1] to the first applications [2,3]. The superior spectral density of synchrotron radiation of the third generation sources allows us now to establish these experiments as a standard technique of hyperfine spectroscopy. The Nuclear Resonance Beamline at ESRF, coming in operation this year, is the first installation dedicated to these purposes. The main direction of the foreseen experiments is an investigation of hyperfine interactions by means of the analysis of the time spectra of resonant nuclear scattering. To meet the corresponding instrumental requirements, the beamline operates with high monochromatic (of about several millielectronvolt bandwidth) and ultrahigh monochromatic (in the order of nanoelectronvolt) beams of X-rays and exploits the time structure and the polarization of the synchrotron radiation. Furthermore, the beamline optics conserves the performance of the X-ray beam, such as high collimation and small beamsize. These features allow extension of the field of application to other domains, like γ-optic, interferometry, crystallography, quasi-elastic and inelastic scattering.

2. General lay-out of the beamline

The beamline lay-out is governed by the concept of supplying external users

with a stable beam of requested nuclear radiation and combining a rapid substitution of experiments with optimal working conditions for each user. The beamline consists of two optics hutches, OH1 and OH2, and three experimental hutches, EH1–EH3 (fig. 1). The beamline optics are sub-divided between OH1 and OH2. The first optics hutch OH1 handles the "white" X-ray beam from the undulator and includes a high heat load monochromator, slit systems, attenuators and energy/intensity monitors. OH2 deals with the monochromatic beam and contains the high resolution monochromators (HRMs), nuclear monochromators and, in a later stage, the focusing elements.

The prepared X-ray beam is supplied into three experimental hutches. EH1 is devoted to resonant nuclear diffraction and contains a standard four-circle diffractometer. EH2 is foreseen for nuclear forward scattering and is equipped with a cryomagnetic system. EH3 is currently reserved for experiments not requiring special equipment. An interlock system allows to carry out an experiment in any of these hutches, while keeping free access into two others. The beam inside these hutches is either transported in shielded vacuum tubes or blocked by the up-stream beam shutter. By this means the experiment in one hutch can be performed in parallel with the preparation work in others. Computers and electronics to run an experiment are located in three separated control cabins (CC1–CC3) next to the corresponding experimental hutches.

To reduce an attenuation of the beam, to avoid small angle scattering and/or inelastic scattering and to suppress the ozone contamination, most of the beamline optics operates in vacuum chambers, consisting of a single vacuum line

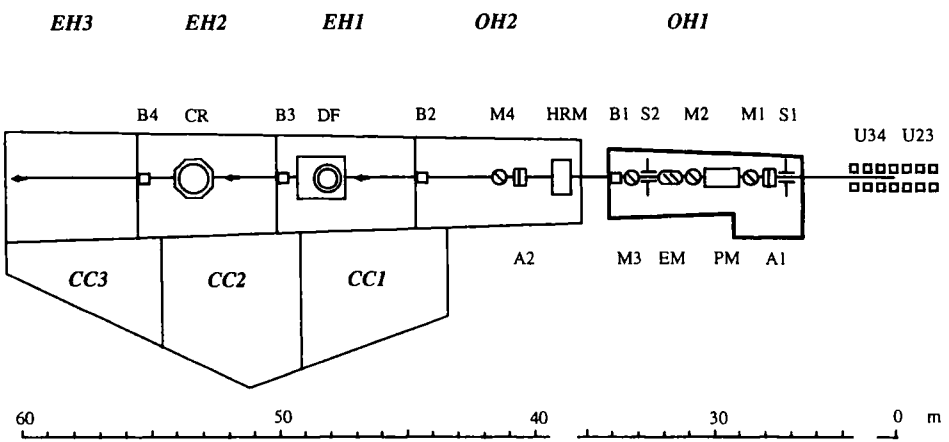

Fig. 1. Schematic lay-out of the Nuclear Resonance Beamline. OH1 – "white" beam first optics hutch; OH2 – second optics hutch; EH1–EH3 – experimental hutches; CC1–CC3 – control cabins; U23 and U34 – 22.8 mm and 34 mm period undulators; S1 and S2 – slit systems; A1 and A2 – attenuators; M1 – timing/intensity monitor; M2–M4 – intensity monitors; PM – double crystal water-cooled fixed-exit Si(111) monochromator; EM – energy monitor; B1–B4 – beam shutters; HRM – high resolution monochromator; DF – 4-circle diffractometer; CR – cryomagnet system.

(10^{-7} Torr) with no windows in between. Presently the vacuum line covers the complete beam path from the source to the high resolution monochromator in OH2 and partly the way from OH2 to EH1. When all attenuators, intensity and energy monitors are open, only Be-windows (700 μm) are in the pass of the beam.

3. Radiation source

3.1. ENERGY

The beamline has two standard ESRF undulators [4] of 22.8 mm (U23) and 34 mm period (U34), installed in a high-β straight section (ID18). Both undulators operate at low-order harmonics. This design provides high flux of the required radiation, keeping the heat load on the monochromator and the background essentially low.

The undulator U23 is optimized for the ^{57}Fe nuclear transition at 14.413 keV in the fundamental. The beam has an energy bandwidth of about 380 eV (FWHM, measured in a cone of 1 × 1 μrad^2), and contains no soft radiation. The total power is only about 50 W (here and below calculated at 100 mA electron current in the storage ring), and the power in the central cone (80 × 80 μrad^2) is about 10 W.

The undulator U34 covers several Mössbauer transitions. Adjustment of the undulator gap allows to tune the fundamental to the resonant energy of ^{181}Ta (6.215 keV) and ^{169}Tm (8.410 keV). The measured energy bandwidth of the radiation is about 180 eV (FWHM). The total power and the power in the central cone are calculated to be 280 and 50 W, respectively. Third harmonics of this undulator can be adjusted to the energies of nuclear transitions in ^{151}Eu (21.5 keV), ^{149}Sm (22.5 keV), ^{119}Sn (23.9 keV) and ^{161}Dy (25.7 keV).

3.2. TIME STRUCTURE

Since the main scope of the foreseen experiments is time resolved nuclear spectroscopy, the timing properties of the X-ray beam are essential for the applications. With a circumference of the storage ring of 844 m one turn of the electrons takes 2817 ns. The frequency of the ESRF radio frequency system is 352.2 MHz, which determines the 2.839 ns spacing between the adjacent buckets, and 992 buckets can be filled.

So far there exist four modes of machine operation [5]. In *multibunch mode*, which is the default mode by now, about 1/3 of the ring circumference is filled. This leads to 352 radiation pulses (equally spaced in time) during 996 ns followed by a 1821 ns gap without radiation. The nominal current is 150 mA with a lifetime of about 60 h.

In *hybrid mode* a single bucket is filled with a current of about 8 mA, and then 1/3 of the ring circumference at the opposite side of the ring is filled with the total

current of about 150 mA like in multibunch mode. Thus the time structure of radiation is analogous to that of the multibunch mode with an additional short pulse in the center of 1821 ns gap. The lifetime of the additional bunch is about 15 h.

In *16-bunch mode* 16 equally spaced buckets are filled with a corresponding spacing of 176.06 ns. The current is limited to about 80 mA and the lifetime of the beam is about 35 h.

Finally, there exists a *single bunch mode* where one bucket is filled with a current of about 15 mA, and a lifetime of about 15 h.

After the completed injection the cleaning process [5] is applied in single bunch, 16-bunch and hybrid modes (in hybrid mode after the single bunch filling). This process eliminates the occasional population of spurious bunches down to 10^{-10} as relative to the main bunch. The typical bunch length is about 110 ps (FWHM) and about 65 ps measured in 16-bunch mode and multibunch mode, respectively [6].

3.3. X-RAY BEAM SIZE AND DIVERGENCE

Due to the different parameters of machine operation, the emittance and consequently the electron and photon beam size and divergence depend on the mode. In 16-bunch mode, which is the favorable mode for the timing applications, the machine is running with a horizontal emittance of $\varepsilon_H = 4$ nm and an 1% coupling. From these values an electron beam size of 54 μm × 0.8 mm (FWHM, here and below given as vert. × hor.) and an electron beam divergence of 4 × 28 μrad^2 may be derived. The divergence of the X-ray beam is 18 × 33 μrad^2, resulting in the beam size of 0.45 × 2.0 mm^2 30 m down stream of the undulator [7].

3.4. POLARIZATION

Another feature which is important for hyperfine spectroscopy is the intrinsic linear polarization of synchrotron radiation. On axis the X-ray beam is 100% linear polarized in the horizontal plane. In the central cone (80 × 80 μrad^2) the polarization is still about 98%. For special applications a polarization up to really 100% ($1-10^{-7}$) can be achieved by means of special crystal optics. Furthermore a polarizer–analyzer system can be introduced.

4. White beam optics

The task of the optics in the OH1 is to handle the heat load of "white" radiation, to define the beam size, to reduce the energy bandwidth of the radiation down to several electronvolts and to monitor the intensity, timing and energy of the beam before supplying it to the OH2.

The high heat-load monochromator is located 30 m downstream of the source and is designed as a double-crystal Si(111) monochromator with fixed exit. The optimization of undulators for low-order harmonics suppresses essentially the

power of the unwanted soft and hard X-rays. This allows to handle the heat load with simple water cooling and provides a long-term stability of crystal positions. In nuclear resonance scattering experiments the monochromator has to deliver over long periods (weeks) the same energy within the rocking curve width. For this purpose the stability of both crystals, especially of the second one, was carefully sought during the monochromator design. The rotation stage, driving the second crystal, is rigidly attached to the base plate and equipped with a high resolution angular encoder (resolution/accuracy 0.17 μrad). Another rotation stage, carrying the first crystal, is moving parallel to the beam to provide fixed exit operation while changing the energy. The crystals are rigidly glued to cooled holders by Wood alloy (proposed by A. Freund, ESRF). Horizontal and vertical positions of the crystals with respect to the beam are controlled by monitoring the footprint of the X-ray beam on the silicon crystal with a CCD camera.

With an offset between entrance and exit beam of 50 mm, which is favorable to minimize the background in the successive experiments, the monochromator covers the energy range from 3 to 30 keV. Alternatively, an offset of 25 mm allows to extend the energy range up to 60 keV.

Commissioning showed the stable performance of the monochromator. At the energy of 14.413 keV the rocking curve width was measured as 30 μrad (FWHM), which should be compared with the theoretical value of 26 μrad. From this value the bandwidth of the supplied radiation can be derived as about 2.8 eV. The flux of 14.413 keV radiation was measured as 3.6×10^{12} photons/s (at 140 mA). Once the monochromator is adjusted, there is no need to re-adjust the angles of both crystals during one week of continuous operation.

The water-cooled slit system upstream the monochromator extracts the radiation of the central cone and reduces the heat load as well as the background. The slit system downstream defines the beamsize for the successive experimental set-up. Intensity monitors are inserted after each "active element" (fig. 1). To exclude windows along the X-ray beam, the permanent use of ion chambers is avoided. Instead of these, the intensity of the beam is monitored by scattering the radiation on removable foils, inserted in the beam inside the vacuum line. Energy calibration is provided by measurements of K- and L-edges of appropriate elements, and can be performed in transmission and/or scattering geometry. A fast detector system facing the "white" beam, based on an avalanche photodiode [8], serves as purity detector and timing control. Several attenuators allow to control the beam flux.

5. Further monochromatization down to millielectronvolt and nanoelectronvolt bandwidth

5.1. HIGH RESOLUTION MONOCHROMATORS

The high resolution monochromators (HRMs) are located in OH2 at 40 m down-

stream of the source. The very compact design is based on two "nested" channel-cut crystals according to an idea in ref. [9]. The HRM has to be tailored for each Mössbauer transition in order to provide highest energy resolution, flux and/or degree of polarization. For 14.413 keV, the transition energy of ^{57}Fe, two sets of HRMs are presently available. One of them operates with an asymmetric Si(4 2 2) and a symmetric Si(12 2 2) channel-cut crystal and delivers a flux of about 1.4×10^9 photons/s (at 150 mA) in an energy bandpass of 5.8 meV. Another one is optimized to supply the radiation with 100% linear polarization and with an energy bandpass of about 7 meV. It contains two Si(8 4 0) channel-cut crystals, which has been proved to be favorable for this purpose. A suppression of the unwanted π-polarized component of radiation by seven orders of magnitude has been achieved [10] with this set-up. Other HRMs for the ^{57}Fe transition as well as for other Mössbauer isotopes are under construction.

In the experiments on resonant nuclear inelastic absorption or inelastic X-ray scattering the energy of radiation, supplied by HRMs, can be tuned within a wide range. A deviation of the energy from the resonance is controlled by angular encoders with resolution of about 0.2 meV (at 14.413 keV). An energy calibration of the HRMs may be carried out using the Bond method [11].

5.2. NUCLEAR MONOCHROMATORS

Normally the degree of monochromatization achieved with HRMs is sufficient to avoid the overload of the detector due to the prompt non-resonant background and to carry out hyperfine spectroscopy. For other experiments, which need a better monochromatization, nuclear scattering has to be used. Resonant nuclear scattering proceeds within a very narrow energy width, so if by some means the non-resonant electronic scattering is suppressed, such nuclear monochromators provide typically energy bandpasses down to neV.

Depending on the application this nuclear monochromator has to be tailored very carefully. For ultra-high suppression of non-resonant background (10^{-7}) pure nuclear reflections are used [1]. Crystals of YIG, $^{57}FeBO_3$ and $^{57}Fe_3BO_6$ are presently available for this purpose. For moderate values of suppression (10^{-3}) multilayers [12] and GIAR films [13] may be chosen.

By default the nuclear monochromators supply a beam at fixed energy. On the other hand for inelastic scattering experiments the energy tunability is a precondition. First approaches of a nuclear monochromator tunable in the microelectronvolt range are just reported [14].

6. Equipment of experimental stations

6.1. DIFFRACTION EQUIPMENT

The main equipment for diffraction experiments is placed in EH1. A standard

four-circle diffractometer with an Eulerian cradle for horizontal scattering geometry is available. By default a resolution of 1.75 μrad for the θ-circle and 17.45 μrad for the other circles is provided. With improved electronics a tenfold better resolution may be achieved. In a later stage the diffractometer will be upgraded to vertical as well as horizontal scattering geometry.

6.2. CRYOGENIC EQUIPMENT

EH2 is devoted to nuclear forward scattering [15] experiments. As in conventional Mössbauer spectroscopy, the experimental set-up is designed for transmission geometry. A cryomagnetic system provides an external magnetic field up to 7 T in horizontal direction, either perpendicular or parallel to the X-ray beam. The variable temperature insert operates in the range from 1.5 to 500 K. The sample volume is a sphere of 50 mm in diameter, which allows e.g. to accommodate high pressure cells. The windows are transparent for X-rays and visible light. The latter is thought e.g. to carry out optical pressure calibration when diamond anvil cells are used. A special feature is an exit window of 60° in the vertical plane for scattering applications.

The temperature range from 20 to 370 K is also accessible with another cryostat, which has a compact closed-cycle design. The cryostat fits to the Eulerian cradle of the four-circle diffractometer, allowing to perform low-temperature measurements under diffraction conditions. The sample chamber design allows to access the whole range of scattering angles. Another sample chamber allows to carry out temperature dependent measurements of inelastic nuclear absorption. A solid angle up to π is accessible for the detector.

6.3. DETECTORS AND ELECTRONICS

The detector systems are based on avalanche photodiodes, which are recently applied to X-rays [8,16]. The choice of the diode is determined by the required time resolution, size and efficiency. The time resolution ranges from 0.1 to 1.0 ns, the size from sub-millimeter diameter up to 16 mm diameter, and the efficiency from several percent to about 50%. The fast timing electronics is based on standard fast NIM modules, including fast ADCs and MCAs. A reference timing signal from the radio frequency system of the machine provides a synchronization of electronics with the electron beam phase.

7. Fields of applications. Preliminary results

The beamline is designed to provide an intense highly monochromatic, collimated and small X-ray beam at the Mössbauer transition energies. Foreseen

experiments cover a wide field of applications, which are classified in table 1. The typical experiments are illustrated below by preliminary results.

7.1. RESONANT NUCLEAR SCATTERING EXPERIMENTS

Synchrotron hyperfine spectroscopy implies the measurements of the splitting or the shift of nuclear levels due to magnetic or electric interaction as well as the orientation of the hyperfine field vector and electric field gradient. Unlike in conventional Mössbauer spectroscopy, the data are obtained by analysis of the time spectra of nuclear scattering. A typical example of the nuclear forward scattering experimental set-up is shown in fig. 2. Short pulses of synchrotron radiation passed through a 10 μm ^{57}Fe foil and excited the 14.413 keV nuclear transition. After a prompt pulse of non-resonant radiation the delayed signal of nuclear scattering in forward direction was measured as a function of time. The time pattern arises from an interference of radiation components with different energies, corresponding to six magnetically splitted sub-levels of ^{57}Fe. The quantum beat period is determined by the splitting, therefore by the hyperfine field. Furthermore, the spectra are sensitive to the direction of the magnetization. In the case of non-magnetized foil

Table 1
Field of applications.

Resonant nuclear scattering
Hyperfine spectroscopy
• *phase transitions*
• *critical phenomena*
• *structure analysis*
Surface study
• *specular surface reflection*
• *conversion electron spectroscopy*
• *multilayers*
General γ-optics
• *basic features of nuclear resonant scattering*
• *multi-beam nuclear diffraction*
Magnetic topography
• *structure of magnetic domains*
Resonant nuclear inelastic scattering
• *energy distribution of nuclear recoil, density of states*
• *Lamb–Mössbauer factor*
High resolution X-ray scattering
Quasi-elastic X-ray scattering, relaxation
Inelastic X-ray scattering
Crystallography
Interferometry

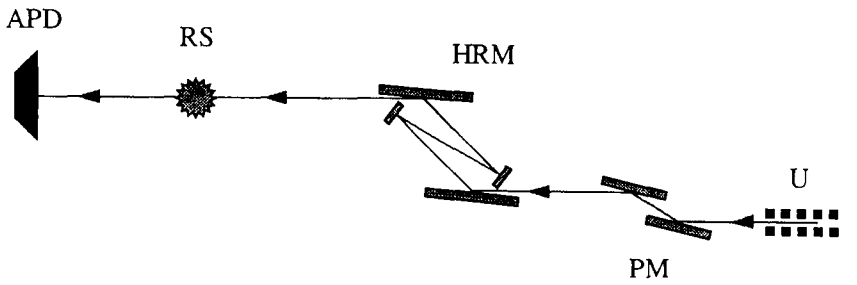

Fig. 2. Set-up for nuclear forward scattering experiment. U – undulator; PM – double crystal water-cooled fixed-exit Si (111) monochromator; HRM – high resolution monochromator; RS – resonant sample; APD – avalanche photodiode detector.

(fig. 3a), where all six nuclear sub-levels are excited, the time spectrum is governed by an interference of all frequencies. When the foil is magnetized horizontally (fig. 3b), only the four $\Delta m = \pm 1$ transitions are excited, a different beat pattern shows up. Finally, when the foil is magnetized vertically (fig. 3c), the interference from the two excited $\Delta m = 0$ transitions results in quantum beats with one frequency. The envelope over the quantum beats is determined by the effective thickness of the sample, allowing the precise measurement of the Lamb–Mössbauer factor.

Typical count rates of these measurements are about 10^3 photons/s, with almost no background (10^{-2} photons/s) in the time window shown. Therefore only a very short time (several minutes) is required for the measurement of a single spectrum. This is especially important for the studies of phase transitions, where numerous spectra have to be taken as a function of temperature, external magnetic field or pressure.

In particular high pressure applications are favorable to be carried out at the Nuclear Resonance Beamline due to the intrinsic small size and low divergence of the beam. As an example, the phase transformation of ferromagnetic α-Fe (bcc lattice) to non-magnetic ε-Fe (hcp lattice) was studied [17]. A non-polarized iron foil of 2.5 μm thickness and about 200 μm diameter was placed in a diamond anvil cell. Spectra between ambient pressure and 34 GPa have been taken (fig. 4). When the pressure is relatively low, the quantum beats are well seen in the spectrum as an indication of iron ferromagnetism. With increasing pressure the contrast of quantum beats becomes smaller and disappears at a pressure of about 21 GPa [18], displaying a transformation of the sample into the non-magnetic phase. Measuring times were less than one hour for one spectrum, which has to be compared with one day measuring time in conventional Mössbauer spectroscopy. In later studies a polarization of the sample by an external magnetic field has been proved to be favorable for the data evaluation [19]. It serves to decrease the number of nuclear transitions involved and to reduce the direction distribution of the hyperfine field.

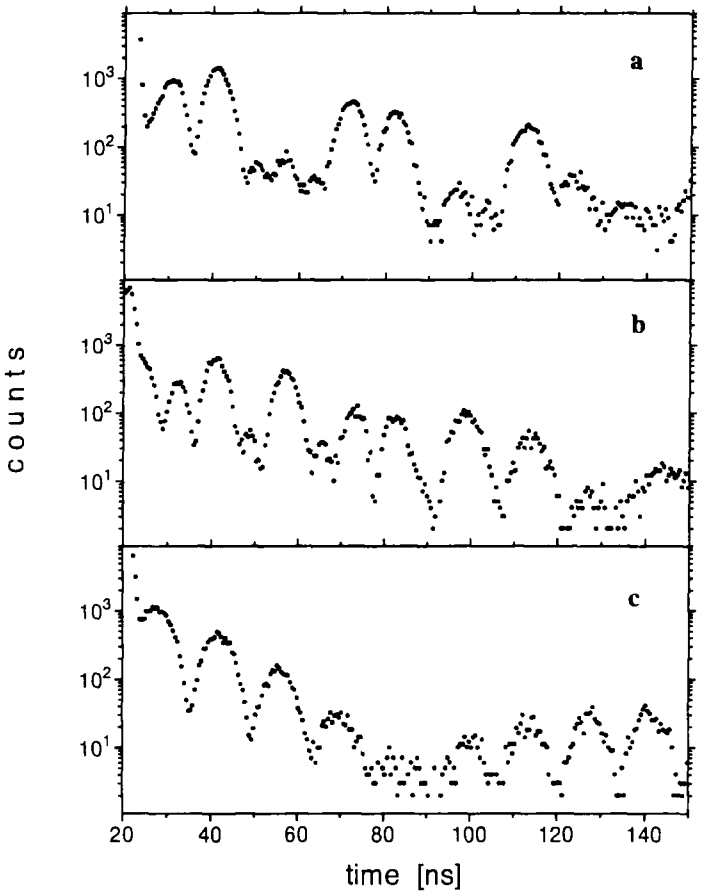

Fig. 3. Time spectra of nuclear forward scattering by 10 μm ^{57}Fe foil under the different conditions of external magnetization: without external magnetic field (a); in horizontal (b) and vertical external magnetic field (c) of 0.1 T.

An example in case of electric interaction, the quadrupole splitting of nuclear levels, is shown in fig. 5. The temperature induced high spin↔low spin transition in $[^{57}Fe(bpp)_2][BF_4]_2$ was studied (the ligand bpp is 2,6-bis(pyrazol-3-yl)pyridine [20]). The sample was 3 mm in diameter. The measurement of each spectrum took about 10 min. At the temperature of about 172 K the sample undergoes an electronic structure transformation. As a result the electric field gradient on the nuclear sites varies, leading to the decrease of the quadrupole splitting with decreasing temperature. The temperature development of both the hyperfine parameters and the Lamb–Mössbauer factor (f_{LM}) was derived from these measurements [21].

The above examples of nuclear forward scattering experiments were performed with 14.413 keV radiation of ^{57}Fe. Furthermore the time spectra of nuclear forward scattering and of conversion electron emission were studied with 8.410 keV

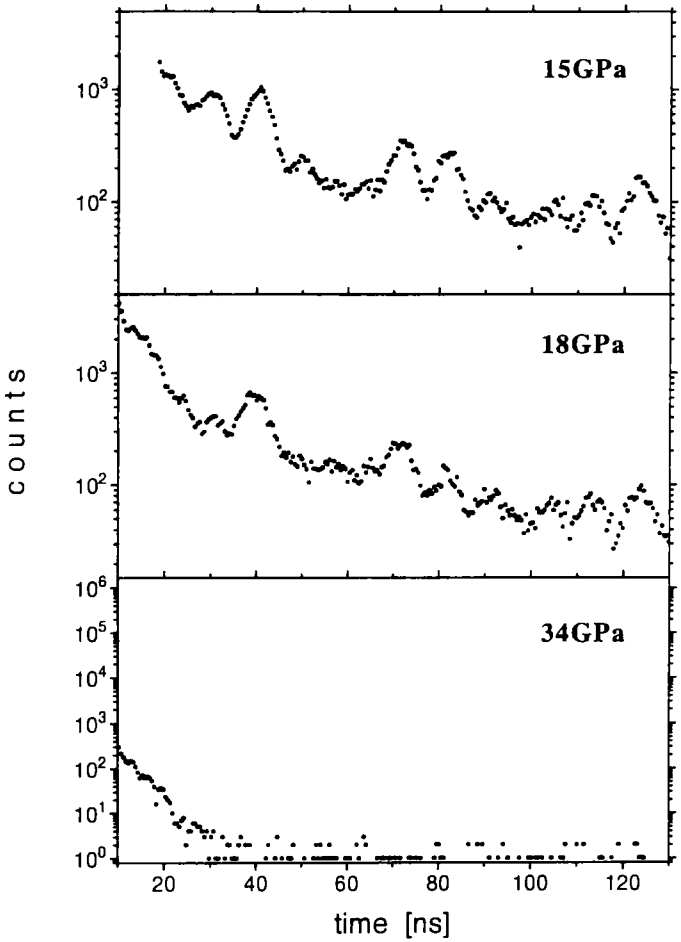

Fig. 4. Time spectra of nuclear forward scattering by 2.5 μm ^{57}Fe foil in a high pressure diamond anvil cell at different pressures.

radiation of ^{169}Tm in case of a TmF_3 sample [22], and nuclear forward scattering of 6.215 keV radiation of ^{181}Ta in a metal Ta foil was observed.

7.2. RESONANT NUCLEAR INELASTIC SCATTERING EXPERIMENTS

A new field has been recently opened in nuclear scattering of synchrotron radiation, namely nuclear inelastic absorption [23]. Resonant nuclear elastic scattering by definition is not accompanied by lattice excitation. Therefore it may leave the nuclei in the sample untouched (i.e. the quantum state before and after the scattering process is the same). In this case it is delocalized over many nuclei, proceeds coherently and is peaked in forward direction. The intensity of nuclear forward

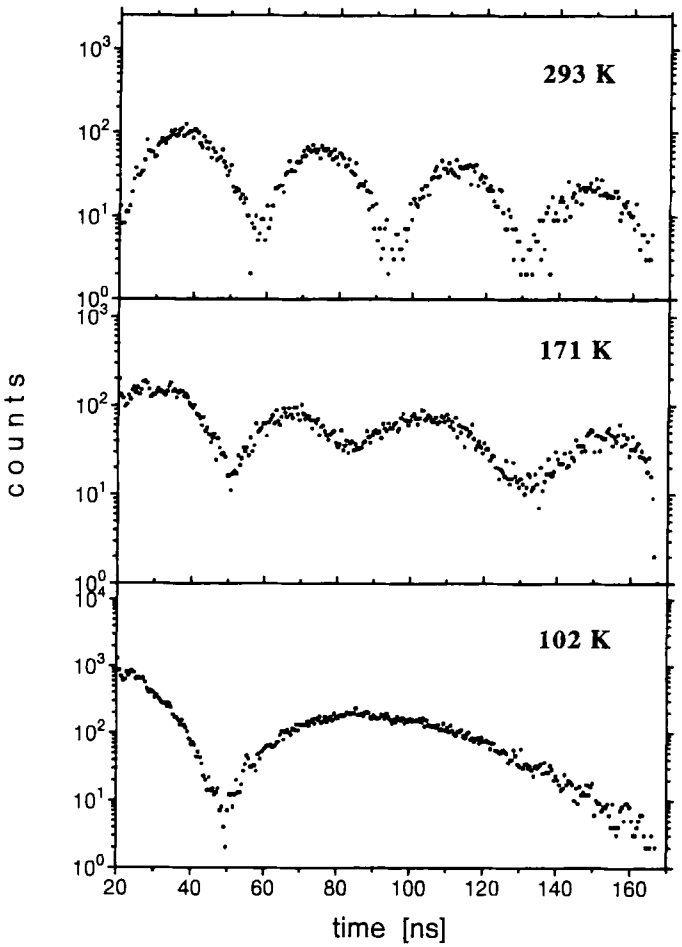

Fig. 5. Time spectra of nuclear forward scattering by $[^{57}Fe(bpp)_2][BF_4]_2$ at different temperatures.

scattering is determined by the recoilless factor f_{LM}. In contrast, nuclear inelastic absorption normally involves the excitation of the lattice. Therefore it is localized on a particular nucleus and proceeds incoherently. This process leads mostly to absorption, not to re-scattering of γ-quanta. The products of nuclear inelastic absorption (with dominating X-ray fluorescence resulting from the internal conversion) are emitted into 4π (incoherent scattering). This channel measures $1 - f_{LM}$.

The continuous energy distribution of the synchrotron light and the superior spectral density of third-generation sources allows to excite the nuclei by radiation, with an energy several millielectronvolts apart of the resonance. The difference is transferred to the phonon excitation of the lattice, and an energy dependence of this process gives the probability of nuclear recoil as a function of transfer energy.

Thus it is possible, for example, to measure at the same time nuclear forward scattering (the part without recoil, "f_{LM}") and the nuclear incoherent scattering (the part with recoil, "$1 - f_{LM}$") i.e. to check the balance of the entire nuclear scattering process.

As an example, the measurements of nuclear inelastic absorption in a ^{57}Fe foil and $[^{57}Fe(bpp)_2][BF_4]_2$ were performed in 18–300 K temperature range. The experimental set-up of a nuclear inelastic absorption experiment is shown in fig. 6. In case of the ^{57}Fe foil (fig. 7) the increase of the recoil probability with increasing temperature is nicely seen. The same holds of course for $[^{57}Fe(bpp)_2][BF_4]_2$ (fig. 8). But in addition this sample shows new features. The energy width of the central peak shows a considerable broadening at room temperature [24]. At temperatures below the phase transformation, that is in the low spin state, a well localized peak of recoil probability with the characteristic energy transfer of about 50 meV arises.

7.3. HIGH-RESOLUTION X-RAY SCATTERING EXPERIMENTS

The Nuclear Resonance Beamline provides a very monochromatic beam of synchrotron radiation. Even after the high resolution monochromator the degree of monochromatization (in case of ^{57}Fe nuclear resonance) is $\Delta E/E = 4.6 \times 10^{-7}$. Furthermore an application of a nuclear monochromator allows to achieve a beam with monochromaticity of about $\Delta E/E = 3 \times 10^{-11}$. It should be stressed that the intensity of this beam is essentially high. For example, the flux from a $^{57}FeBO_3$ nuclear monochromator set to the (333) pure nuclear reflection was measured as 7×10^4 photons/s (at 100 mA). The longitudinal coherence length of this beam is about 3 m. An application of such a beam in interferometry may be quite attractive.

The availability of such beams allows to establish nuclear radiation as a new standard of wavelength in the hard X-ray region, giving a reliable reference for crystallography. Besides that, the stable energy of nuclear levels and its narrow

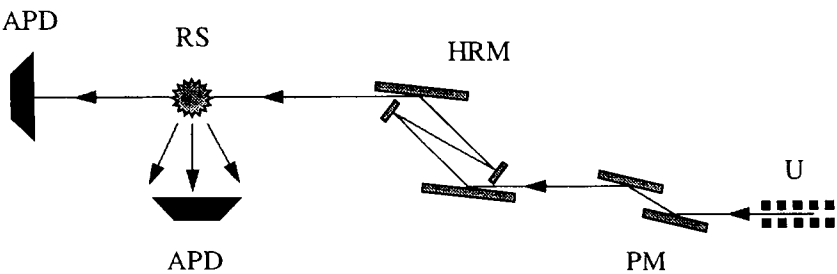

Fig. 6. Set-up of resonant nuclear inelastic absorption experiment. U – undulator; PM – double crystal water-cooled fixed-exit Si(111) monochromator; HRM – high resolution monochromator; RS – resonant sample; APD – avalanche photodiode detector.

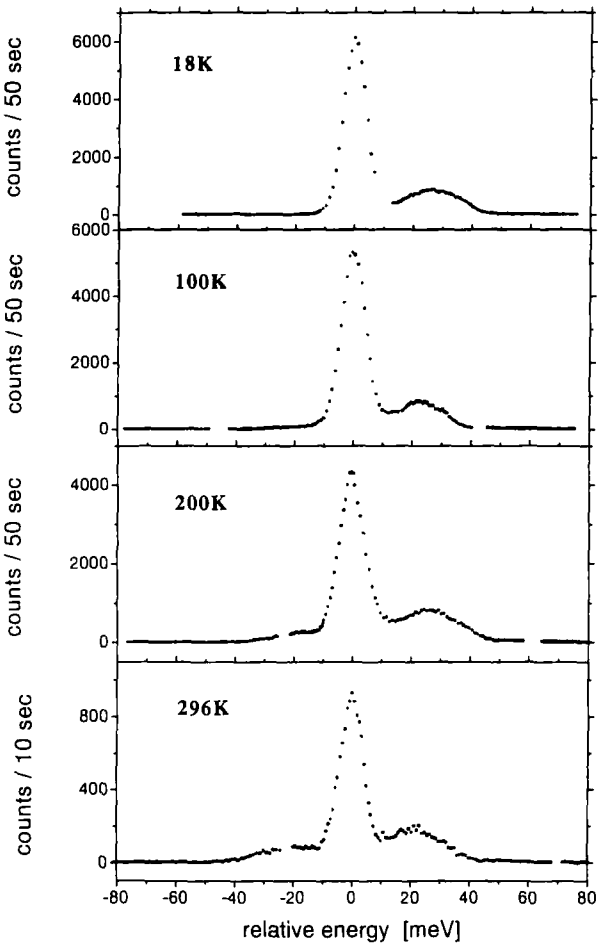

Fig. 7. Energy spectra of resonant nuclear inelastic absorption in 20 μm ^{57}Fe foil at different temperatures.

widths provide a base to use nuclear levels for energy analysis, for example, of inelasticaly scattered X-rays. The corresponding studies are presently carried out at the Nuclear Resonance Beamline.

8. Conclusion

After the first few weeks of commissioning the Nuclear Resonance Beamline has already proved to be an excellent tool not only for hyperfine spectroscopy but also for a wide variety of connected applications. The outstanding properties of the X-ray beam will give new impetus to fields like high pressure, inelastic scattering, time resolved reactions, diffraction. Access to the facility is governed by means of

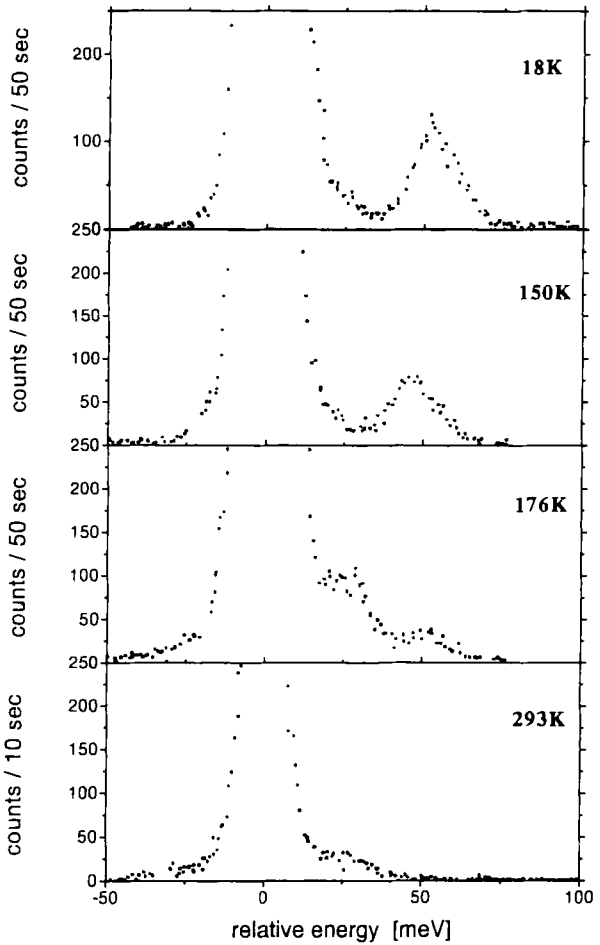

Fig. 8. Energy spectra of resonant nuclear inelastic absorption in $[^{57}Fe(bpp)_2][BF_4]_2$ at different temperatures.

proposals. Twice a year, on 1st March and 1st September, proposals have to be submitted and the available beamtime is allocated to the proposers by the recommendation of review committees [#1].

Acknowledgement

The support of all services of the ESRF to the construction and the set-up of the beamline is highly acknowledged. The commissioning and the measurements were performed by the Nuclear Resonance Group (A.Q.R. Baron, J. Ejton,

[#1] For more information one may look in the World Wide Web (http: //www.esrf.fr).

H. Grünsteudel [#2], H.F. Grünsteudel, Z.Hubert, S.Kishimoto [#3], H.J.Rasmussen) in collaboration with H.-J.Hesse [#4], O.Leupold [#5], J.Metge [#5], Yu.V.Shvyd'ko [#5] and G.Wortmann [#4]. The continuous support by E. Gerdau [#5] is highly acknowledged.

References

[1] E. Gerdau, R. Rüffer, H. Winkler, W. Tolksdorf, C.P. Klages and J.P. Hannon, Phys. Rev. Lett. 54 (1985) 835.
[2] E. Gerdau and U. van Bürck, in: *Resonant Anomalous X-ray Scattering. Theory and Applications* eds. G. Materlik, C.J. Sparks and K. Fischer (Elsevier, Amsterdam, 1994) p. 589.
[3] G.V. Smirnov, Proceedings of this conference, Hyp. Int. 97/98 (1996) 551.
[4] P. Elleaume, Nucl. Instr. Meth. A 266 (1988) 125.
[5] J.-L. Revol, E. Plouviez and R. Rüffer, Synchrotron Radiation News 7(4) (1994) 23.
[6] K. Scheidt, private communication.
[7] L. Farvacque, J.L. Laclare, C. Limborg and A. Ropert, ESRF Newsletter 24 (1995) 12.
[8] S. Kishimoto, Nucl. Instr. Meth. A 309 (1991) 603.
[9] T. Ishikawa, Y. Yoda, K. Izumi, C.K. Suzuki, X.W. Zhang, M. Ando and S. Kikuta, Rev. Sci. Instrum. 63 (1992) 1015.
[10] U. Bergmann, D.P. Siddons and J.B. Hastings, in: *Resonant Anomalous X-ray Scattering. Theory and Applications*, eds. G. Materlik, C.J. Sparks and K. Fischer (Elsevier, Amsterdam, 1994) p. 619.
[11] W.L. Bond, Acta Cryst. 13 (1960) 814.
[12] A.I. Chumakov, G.V. Smirnov, A.Q.R. Baron, J. Arthur, D.E. Brown, S.L. Ruby, G.S. Brown and N.N. Salashchenko, Phys. Rev. Lett. 71 (1993) 2489.
[13] R. Röhlsberger, E. Gerdau, M. Harsdorff, O. Leupold, E. Lüken, J. Metge, R. Rüffer, H.D. Rüter, W. Sturhahn and E. Witthoff, Europhys. Lett. 18 (1992) 561.
[14] R. Röhlsberger, E. Gerdau, W. Sturhahn, E.E. Alp and R. Rüffer, in: *Proc. Int. Conf. on the Applications of the Mössbauer Effect*, Rimini 1995.
[15] J.B. Hastings, D.P. Siddons, U. van Bürck, R. Hollatz and U. Bergmann, Phys. Rev. Lett. 66 (1991) 770.
[16] A.Q.R. Baron and S.L. Ruby, Nucl. Instr. Meth. A 343 (1994) 517.
[17] H.F. Grünsteudel, H.-J. Hesse, A.I. Chumakov, H. Grünsteudel, O. Leupold, J. Metge, R. Rüffer and G. Wortmann, Proc. of this conference.
[18] R.D. Taylor, M. Pasternak, R. Jeanloz, J. Appl. Phys. 69 (1991) 218.
[19] H.F. Grünsteudel et al., to be published.
[20] H.A.Goodwin and K.H.Sugiyarto, Chem. Phys. Lett. 139 (1987) 470.
[21] H. Grünsteudel et al., to be published.
[22] S.Kishimoto et al., to be published.
[23] M. Seto, Y. Yoda, S. Kikuta, X.W. Zhang and M. Ando, Phys. Rev. Lett. 74 (1995) 3828; W. Sturhahn, T.S. Toellner, E.E. Alp, X. Zhang, M. Ando, Y. Yoda, S. Kikuta, M. Seto, C.W. Kimball and B. Dabrowski, Phys. Rev. Lett. 74 (1995) 3832.
[24] A.I. Chumakov, R. Rüffer, H. Grünsteudel, H.F. Grünsteudel, G. Grübel, J. Metge, O. Leupold and H.A. Goodwin, Europhys. Lett. 30 (1995) 427.

[#2] Medizinische Universität zu Lübeck.
[#3] Photon Factory, National Laboratory for High Energy.
[#4] GHS - Universität Paderborn.
[#5] Universität Hamburg.